Environmental Science Processes & Impacts

ROYAL SOCIETY OF CHEMISTRY

PAPER

View Article Online
View Journal | View Issue

Cite this: *Environ. Sci.: Processes Impacts*, 2022, **24**, 1923

Changes in light absorption and composition of chromophoric marine-dissolved organic matter across a microbial bloom†

Michael R. Alves, [a] Elizabeth K. Coward,[a] David Gonzales,[a] Jon S. Sauer, [a] Kathryn J. Mayer, [ab] Kimberly A. Prather [ac] and Vicki H. Grassian *[a]

Received 10th April 2022
Accepted 22nd August 2022

DOI: 10.1039/d2em00150k

rsc.li/espi

Marine chromophoric dissolved organic matter (m-CDOM) mediates many vital photochemical processes at the ocean's surface. Isolating m-CDOM within the chemical complexity of marine dissolved organic matter has remained an analytical challenge. The SeaSCAPE campaign, a large-scale mesocosm experiment, provided a unique opportunity to probe the *in situ* production of m-CDOM across phytoplankton and microbial blooms. Results from mass spectrometry coupled with UV-VIS spectroscopy reveal production of a chemodiverse set of compounds well-correlated with increases in absorbance after a bacterial bloom, indicative of autochthonous m-CDOM production. Notably, many of the absorbing compounds were found to be enriched in nitrogen, which may be essential to chromophore function. From these results, quinoids, porphyrins, flavones, and amide-like compounds were identified *via* structural analysis and may serve as important photosensitizers in the marine boundary layer. Overall, this study demonstrates a step forward in identifying and characterizing m-CDOM using temporal mesocosm data and integrated UV-VIS spectroscopy and mass spectrometry analyses.

Environmental significance

Marine chromophoric dissolved organic matter has been characterized and correlated with the optical absorption of different classes of compounds.

Introduction

The photoactive, or chromophoric, subset of marine dissolved organic matter (referred to here as marine chromophoric dissolved organic matter, m-CDOM), is a ubiquitous constituent of one of the largest global carbon (C) reservoirs and the greatest pool of reduced carbon (~660 PgC) in marine environments.[1] Capable of performing direct and indirect photochemical processes in the environment,[2,3] and driving the amount of UV-radiation and visible light absorption at the ocean's surface,[4] m-CDOM is thought to be a complex mixture of compounds derived from both allochthonous and autochthonous sources, such as phytoplankton and bacterial blooms.[5–9] The composition and structures of m-CDOM drive an extensive array of photochemical reactions and metabolomic pathways catalyzed by solar radiation in the photic zone,[10] including potential light-driven production of nitrous acid (HONO) – an important atmospheric oxidant.[11,12] Despite the importance of speciation in modulating behavior, the molecular composition of m-CDOM has yet to be elucidated.

Much of this uncertainty is rooted in the diverse production pathways of m-CDOM, identification limitations within the broader chemical complexity of marine organic matter, and the inherent photo-reactivity of such compounds.[13,14] Characterizing natural organic matter is universally a complex analytical endeavor, given the number and chemodiversity of compounds that make up these samples across different environments.[15,16] As such, a synchrony of different techniques, such as nuclear magnetic resonance (NMR) spectroscopy and high-resolution mass spectrometry (HRMS), are required to detect and characterize discrete DOM populations.[17–21] Identification of m-CDOM compounds, more specifically, within bulk marine DOM has largely been accomplished using other approaches such as excitation-emission matrices (EEMs), which do not provide the molecular-level resolution critical to understanding and predicting m-CDOM behavior in marine systems.[22] Some studies

[a]*Department of Chemistry and Biochemistry, University of California San Diego, La Jolla, California 92093, USA. E-mail: vhgrassian@ucsd.edu*

[b]*Department of Chemistry, Colorado State University, Fort Collins, Colorado, 80523, USA*

[c]*Scripps Institution of Oceanography, University of California San Diego, La Jolla, California 92093, USA*

† Electronic supplementary information (ESI) available. See https://doi.org/10.1039/d2em00150k

have attempted to separate m-CDOM based on assumed structure composition (*e.g.* aromatic content) and incorporate mass spectrometry in conjunction with spectroscopic measurements.[23] However, results are limited to characterizations based on formulaic assignments and potential functionality.

This work aims to isolate and characterize m-CDOM formation at the molecular level using integrated absorbance measurements and mass spectrometry during sequential microbial blooms within a large-scale mesocosm flume. The sequential exponential growth of phytoplankton, which reduce CO_2 from their surroundings, and subsequent marine bacterial growth from decayed substrates,[24,25] is a documented autochthonous pathway of m-CDOM production.[26,27] Thus, organic matter composition was characterized throughout a large-scale (12 000 L wave channel) mesocosm experiment, the 2019 Sea Spray Chemistry and Particle Evolution (SeaSCAPE) study at Scripps Institution of Oceanography throughout sequential phytoplankton and bacterial blooms under controlled conditions.[28] Using integrated UV-VIS spectroscopy and high-resolution mass spectrometry to characterize changes in organic matter composition over time, this work aims to provide insight into the composition of m-CDOM, a critical but understudied photochemical driver in the surface ocean. Ultimately, this research also attempts to search for a molecular model, or models, of m-CDOM, to support future fundamental photochemical studies.

Experimental methods

SeaSCAPE wave channel and experimental design of microbial bloom

The collaborative SeaSCAPE 2019 campaign project, which aimed to characterize realistic ocean-atmosphere chemistry during microbial blooms in a wave channel, has been previously detailed by Sauer *et al.*, 2021.[29] Briefly, approximately 11 800 L of seawater (33.8 PSU) was collected from Ellen Browning Scripps Memorial Pier in La Jolla, California (32.8663° N, 117.2546° W) and immediately filtered to 50 microns to remove the majority of non-microbial biota and large grazers. The filtered seawater was then transferred into a cleaned glass wave channel and allowed to equilibrate at ambient temperature for 24 hours. An electromagnetically driven paddle was used to generate waves down the 33 meter wave channel onto an artificial beach made of fiberglass. Nutrients were then added to the wave channel and fluorescent lights (Spectra 5700K F32-T8, Full Spectrum Solutions, Inc.) were installed along the walls of the flume to support a diurnal light cycle. Three separate microbial blooms were studied during this campaign project, though only the third one, which lasted for 23 days, will be the focus of this study. The wave flume was cleaned and rinsed with acetic acid and Milli-Q, and refilled with seawater from Scripps Pier, between each bloom. This experiment observed two distinct microbial blooms, a first proliferation of phytoplankton species followed by a second largely bacterial bloom, as viral contributions were also observed. A more comprehensive description of the biodiversity and population dynamics during the SeaSCAPE campaign can be found in Sauer *et al.*, 2021 and a schematic is provided in ESI (Scheme S1†).[29]

m-DOM isolation and purification

At eight intervals over the course of 23 days in July and August of 2019, 20 L of water was collected from the flume channel. Sampling occurred on T0, T2, T6, T9, T13, T16, T19, and T22 in which samples are denoted by the numbers of days passed from start corresponding to July 24th, 26th, 30th, and August 2nd, 6th, 9th, 12th, and 15th respectively. All materials used to collect each sample, such as the polypropylene carboy, PTFE-lined tubing, and filters, were pre-rinsed with HPLC-grade methanol (MeOH) and Milli-Q water three times before each collection. Glassware used for the last step of the extraction had an additional step of combustion (500 °C for 7 hours) before use. The carboy was additionally rinsed inside with water from the wave channel 3× before being filled to a pre-measured 20 L mark. From each of these eight 20 L samples, dissolved organic matter (DOM) was isolated *via* sequential filtration through 10 μm nylon mesh, 0.7 μm (pre-combusted glass fiber filters), and 0.2 μm filters (polyethersulfone, 47 mm, MilliporeSigma), maintaining a pressure below 5 psi to avoid lysing any cells present. After filtration, the seawater was acidified to pH 2 using 1 M HPLC-grade HCl (Fisher Scientific) to remove any inorganic carbon contributions[30] and increase sample interaction with the resin by protonation.

The resultant DOM was purified *via* solid-phase extraction (SPE) as described by Dittmar *et al.*,[31] using 5 g Priority PolLutant (Bond Elut PPL, Agilent) cartridges. With the cartridges having a max loading of 50 L of seawater, the loading of m-DOM onto the SPE cartridges was kept under 10 L per gram of absorbing material, and concentration of m-DOM throughout the mesocosm experiment did not exceed 2 mg C L^{-1}. The DOM eluent, with methanol, post-SPE processing was dried in a rotary evaporator and then stored in a freezer at −21 °C prior to further analyses. Samples collected for tandem mass spectrometry (MS2) analysis, later described, were collected in a similar fashion in parallel.

Elemental characterization of dissolved C

Analysis of dissolved organic carbon (DOC) concentrations have been previously reported by Sauer *et al.*, 2021 across the entire bloom experiment.[29] Briefly, duplicate 40 mL aliquots of flume seawater were collected at each sampling interval and filtered into combusted glass vials through a 0.7 μm Whatman GF/F filter. Filtrate samples were immediately acidified to pH 2 with concentrated HCl prior to analysis on a Shimadzu TOC-VCSH catalytic combustion oxidation instrument.

Absorbance characterization and spectral slope derivation

Absorbance spectra were also collected from all temporal SPE extract samples using a Shimadzu UV-3600 UV-VIS-NIR spectrophotometer using a 1 cm quartz cuvette. For each sample, 4 mL of m-DOM in MeOH were isolated and analyzed across wavelengths ranging from 250 to 700 nm. The samples were not diluted into water to minimize sample handling and maximize

signal of the chromophores. The samples were diluted to equal concentrations by mass of the m-DOM to obtain the mass attenuation coefficient (MAC). Absorbance spectral slopes for each sample were also calculated for the wavelength ranges of 275–295 nm ($S_{275-295}$) and 350–400 nm ($S_{350-400}$) *via* a single exponential decay function, a_l (eqn (1)), by nonlinear regression, as reported in Helms *et al.*, using SigmaPlot software (SPSS Inc.),[32]

$$a_l = Ae^{-S(l - l_{ref})}, \quad (1)$$

where, A is amplitude or concentration, S (nm^{-1}) is the spectral slope, and l is the wavelength. Slope values over these discreet spectral ranges have been previously shown to directly correlate with DOM degradation and molecular weight.[32]

High-resolution mass spectrometry and post-processing

The molecular compositions of all SPE eluent samples were characterized *via* Orbitrap mass spectrometry (Thermo Fisher Scientific). The Orbitrap was externally calibrated for mass accuracy and tuned on the day of analysis using the manufacturer's guidelines and a standard calibration solution (Pierce ESI Ion Calibration Solutions, Thermo Fisher Scientific). A solvent blank and a method blank, where the SPE PPL was used with methanol and no sample, were utilized for blank subtractions. Additionally, the spectra were internally calibrated using persistent known compounds across a mass range from 150 to 1500 m/z. Samples were resuspended in MS-grade MeOH to a concentration of 0.5 mg mL^{-1} by mass m-DOM, and loaded to the heated electrospray ionization (HESI) through direct injection at a flow rate of 5 μL min^{-1}. After negative mode ionization, ions were then transferred into a linear ion trap and subsequently the Orbitrap cell. Broad-band mass spectra were then recorded between 150 and 1500 m/z with a mass resolution of 240 000 (at m/z 200). A total of 120 scans were accumulated, and subsequent m/z, intensity, and resolution data for all peaks were exported to individual mass lists.

After analysis, only m/z values with a signal-to-noise ratio (S/N) ≥ 10 were exported for formula assignment. As previously published,[33,34] empirical formula matches were assigned to all resolved peaks within the bounds of $C_{1-50}H_{1-100}O_{1-30}N_{0-5}S_{0-2}P_{0-2}$, and molecular formula were assigned based on the following: (1) Kendrick mass defect analysis, (2) least number of nonoxygen heteroatoms, and (3) lowest parts per million m/z deviation, with calculated theoretical m/z values of the assigned formulae within an error value of ≤0.5 ppm of measured m/z values. Over 10 000 molecular formulae were assigned amongst all samples, which were further binned into assigned compound classes according to elemental ratios and a modified aromaticity index (AI_{mod}), shown in eqn (2).[35]

$$AI_{mod} = (1 + C - 0.5O - S - 0.5H)/(C - 0.5O - S - N - P), \quad (2)$$

Compound classes were assigned as follows: condensed polycyclic aromatics ($AI_{mod} > 0.66$), polyphenols ($0.66 \geq AI_{mod} > 0.50$), highly unsaturated ($AI_{mod} \leq 0.50$ and $H/C < 1.5$), aliphatic compounds ($2.0 \geq H/C \geq 1.5$) with (+N) or without (−N) nitrogen, and saturated compounds ($H/C > 2$). Lastly, compounds present in only one sample were removed from further analyses, including compound class statistics, heteroatomic content calculations, and Spearman's rank correlations.

Spearman's rank correlations

Spearman ranking is a statistical measure of the dependence between two non-parametric variables. In this study, we correlate absorption parameters to sum-normalized compound intensities derived from Orbitrap mass spectrometry. Within each of the sample timepoints T0–T22, contains a bulk UV-VIS spectrum and a direct-HRMS measurement of the intensities for each observed, and assigned, molecular formulae. Taking the entire experiment into account, a specific formula may increase, decrease, or remain relatively unchanged in intensity throughout T0–T22. A change in UV-VIS parameters can be treated similarly. This statistical analysis assigns ranks (*e.g.*, 1, 2, 3,…) to each point depending on their value and compares the similarity of these two now-ranked datasets. Having the same rank across each timepoint from both datasets would result in a Spearman rank correlation of 1. This type of analysis is useful in comparing measurements that may not always be linear, such as those related to highly complex mechanisms like the formation of DOM *via* various metabolic and chemical pathways. This type of analysis would not be ideal if the datasets were large or something resembling a distribution, as this ranking correlation relies on assigning ranks to each value as the relationship increases or decreases. Only correlations in compounds present in at least 6 out of 8 timepoints were considered for this study.[36,37] Correlations were deemed significant if they had a p-value ≤ 0.05, and those presented as positively well-correlated were of R values that range from 0.5 to 1.0, the latter being the maximum value.

Results and discussion

Evolution of m-DOM absorbance during sequential biotic blooms

Changes in m-DOM concentration (*i.e.*, all of the marine dissolved organic matter, as [DOC], and not just the light absorbing component), absorbance, and potential m-CDOM production were measured throughout a microbial bloom progression (Fig. 1 and 2). As noted in Sauer *et al.*, 2021,[29] DOC steadily increased in concentration throughout the experiment, due to both primary and bacterial production, consistent with previous bloom incubation experiments.[38,39] The phytoplankton populations experienced a growth phase during the first week of wave channel operation (T6), followed by abrupt decay (T9), represented by Chla concentrations (Fig. 1b). Subsequent rapid growth in bacterial biomass was observed, reaching peak cell counts at T13 before declining at the conclusion of experimental operations (T22) (Fig. 1c). Absorbance increased over the experimental time course, with a marked increase observed after peak bacterial growth at T13 (Fig. 1c), suggesting the production of chromophoric

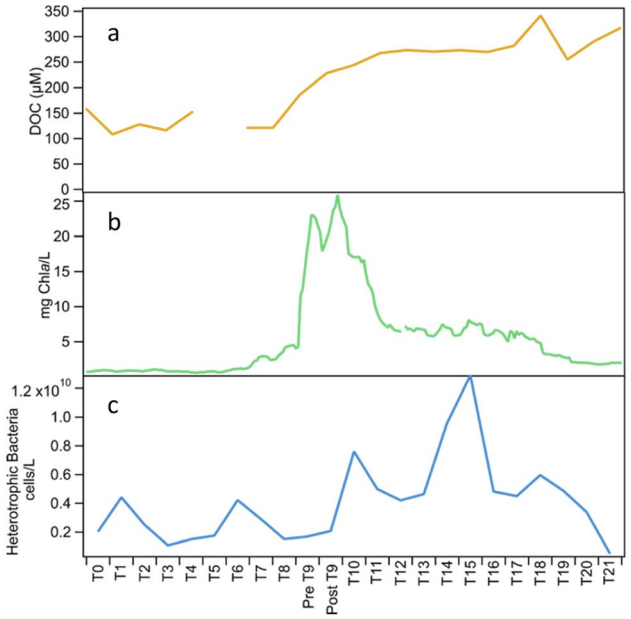

Fig. 1 (a) Dissolved organic carbon measurement by TOC analysis *via* combustion catalytic oxidation, (b) chlorophyll a concentration, and (c) heterotrophic bacterial cell counts per liter of seawater. This data has been replotted and reproduced from ref. 29 with permission from the Royal Society of Chemistry.

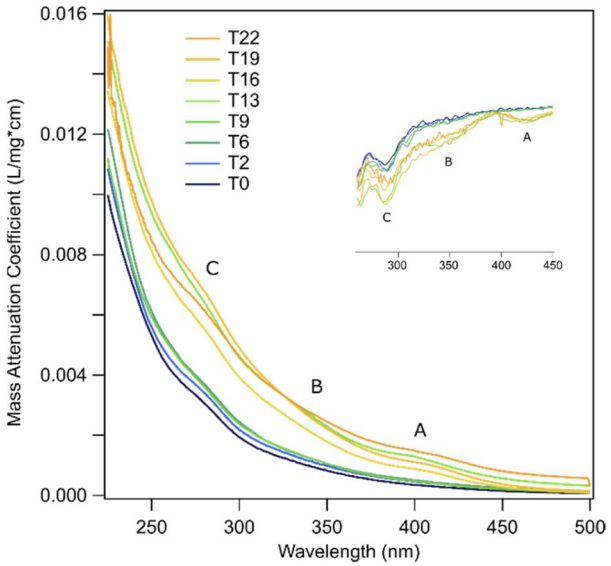

Fig. 2 Mass attenuation coefficient spectrum of m-DOM samples in methanol, calculated from the UV-VIS spectra, collected from the SeaSCAPE Bloom 3 experiment (from T0 to T22, where T0 = time zero). All spectra were taken dissolved in methanol. Samples were dissolved to a standard mass concentration of the extracted m-DOM (mg of m-DOM). (Inset) The inset spectra show the 1st derivative of the m-DOM to better identify the A, B, and C peaks that are contributing to the broad spectrum.

compounds *via* microbial mineralization of phytoplankton biomass, as previously observed by Kinsey *et al.*, 2018.[26] The use of SPE-PPL to extract this m-DOM limits the scope of the extracted pool of compounds observed in this study. Extraction efficiencies for marine DOM are reported to be between 40 and 50% for marine DOM.[31] SPE must be used for m-DOM for two reasons, to concentrate the sample due to the naturally low amount in marine environments and to remove the large amount of salt present.[31] In many cases, this DOM is reported as "SPE-DOM", however, to simplify the nomenclature here, m-DOM and m-CDOM are used instead.

Specifically, three distinct spectral regions – 280, 350, and 410 nm – displayed enhanced absorbance denoted by peaks C, B, and A respectively (Fig. 2). Shoulders at 280 and 350 nm were seen throughout the entire experiment, becoming more distinct over time. This behavior is consistent with spectroscopic measurements of microbial growth in laboratory and field experiments.[40] A distinct peak at 410 nm only appears during and after the microbial bloom peak, persisting throughout the bloom time course. Absorbance at 410 nm, the A peak, has only infrequently been observed in prior examinations of m-CDOM, and previously only appears after peak microbial growth, suggesting the associated compounds are likely produced biotically.[41,42] In theoretical work by Karimova *et al.* 2021, this A peak has been proposed to partially arise from electronic transitions of saturated carbon chains with diol- and oxy-groups near an aromatic center, though additional experimental work is needed to validate such proposed structures.[43] The C peak, at 280 nm and higher energy wavelengths, is associated with aromatic rings and aromaticity in general, particularly $\pi > \pi^*$ transitions. The B peak, at 350 nm, is commonly associated with an $n \rightarrow \pi^*$ transition but can also overlap with nearby $\pi \rightarrow \pi^*$ transitions.[43] This broad peak can be composed of light absorption from peptides, amino acids, flavins, tannins, *etc.*[44,45] However, as noted above, this subset is vastly uncharacterized. It should be noted that due to the nature of the sample, it is unlikely that aggregates and thus absorption related to the charge transfer model are represented here.[46] These clusters are likely important in the makeup of CDOM and should be further studied through the use of complementary techniques.

Integrated UV-VIS spectroscopy and HRMS: signatures of CDOM production

We integrated spectroscopic analyses with high-resolution Orbitrap mass spectrometry to isolate the production of m-CDOM within broader shifts in m-DOM chemodiversity. Within the 10 000+ unique formulae identified, relative abundance within the compound classes assigned did not vary significantly over the course of the experiment (Table S1 and ESI Fig. S1†). We hypothesize that this is likely due to the fact that changes in molecular composition due to external processes are not often reflected in changes in the compound classes themselves, particularly in large complex and dynamic experiments such as this mesocosm. Broader shifts in heteroatom content (Fig. S2A†), HRMS-derived molecular weight (MW; Fig. S2B†), and aromaticity (calculated using eqn (2) and see Fig. S2C†), were observed as microbial populations, and thus metabolic pathways. Notably, after the peak bacterial cell counts, m-DOM

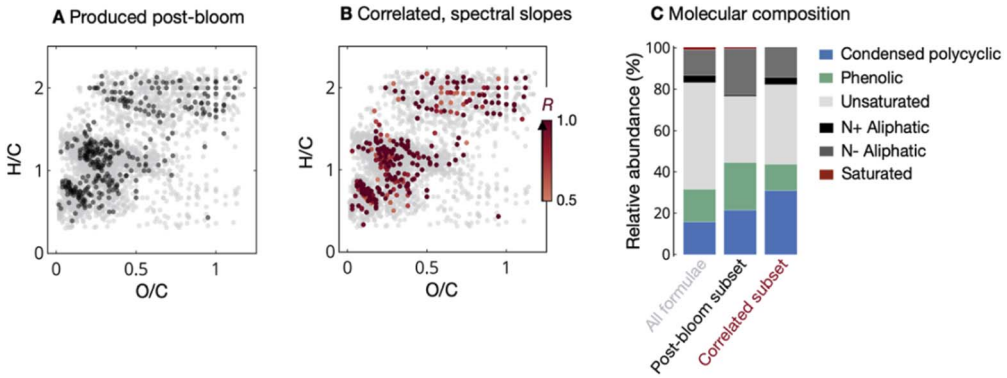

Fig. 3 van Krevelen diagrams (A and B), in which each dot represents molecular formulae, identification of compounds produced post-bacterial bloom (A, black), and those positively correlated with spectral slopes $S_{275-295}$ and $S_{350-400}$, with R values ≥ +0.5 (B, color scale) overlaid on all compounds identified for reference (light grey). The relative molecular composition of all compounds, the subset produced post-bloom, and the subset correlated with spectral slope values is shown in (C).

was highly enriched in N, depleted in sulfur (S), and of greater aromaticity than before the bacterial bloom.

Amidst observed m-DOM chemodiversity dynamics, predicted m-CDOM production was estimated through (i) identification of new compounds produced post-bacterial bloom peak, and (ii) Spearman's ranking correlations between each compound's relative abundances across the experiment and absorbance parameters collected from each m-DOM sample (Fig. 3), thus generating a pool of different chromophores and light absorbing molecules. Indices of absorbance used were the intensity of absorption at 410 nm, ε_{410}, and simple exponential fits of spectra between 275–295 nm ($S_{275-295}$) and 350–400 nm ($S_{350-400}$) (eqn (1)), which can be reflective of photochemically induced shifts in MW and degradation (see Methods for further details).[47] Of the 2000+ formulae assigned and filtered, 397 were produced after the bacterial bloom peak (T16) and observed in all subsequent timepoints (T16–T22, Fig. 3A). Spearman's ranking, considering compounds present in at least 75% of samples, indicated strong overlap between those bacterially-produced (Fig. 3A) and photoactive (Fig. 3B) populations identified as exhibiting positive correlation coefficients with both $S_{275-295}$ and $S_{350-400}$ ($R \geq +0.5$ observed between each formula and spectral slope value, mean R value presented), evident in van Krevelen space. A molecular compound in the van Krevelen space is defined by it oxygen : carbon and hydrogen : carbon ratios and is commonly used in DOM literature to visualize chemical character and possible reactive pathways.[36] A list of the positively and negatively correlated compounds in this subset can be found in the ESI (Table S2†). Overlap in the C and B peaks (Fig. 2) result in a high similarity of correlated molecular formulae, while the A peak remained as a mostly distinct set of formulae (ESI Fig. S3†). Such photoactive compounds ($n = 282$) represented an increasingly aromatic subset, in agreement with previously published findings of m-CDOM aromaticity and chromophore signatures (Fig. 3C).[48] However, all subsets contained compounds across all structural classes, suggesting that m-CDOM is even more chemodiverse than previously considered.[22] Additional mesocosm-like experiments such as the one presented here could shed light on the uniqueness, or lack thereof, of m-CDOM across different biospheres.

Notably, the population of compounds well-correlated in intensity to absorbance values, thus thought to encompass m-CDOM, were also found to be enriched in nitrogen (N) (Table 1). The carbon-nitrogen ratio C/N of all MS-identified DOM was calculated, weighted by MS intensity, to be 13, similar but slightly lower compared to past studies, where numbers have largely been reported between 14 and 20 in the Pacific Coastal surface waters and southern California coastal regions.[49,50] The formulae found in the subsets $S_{350-400}$, $S_{275-295}$, and ε_{410}, in contrast, displayed significantly lower weighted C/N ratios of 8.6, 7.2, and 8.0, respectively. The enrichment of N-containing compounds, evidenced by decreases in C/N, in photo-active subsets suggests preferential incorporation of N during the formation of chromophores. Because this elemental analysis is done using HESI-MS negative mode, these values are not directly comparable to the study referenced. However, the relative change and estimate of N is interesting in of itself for the purpose of this study. This enrichment of N appears element-specific, as H/C and O/C ratios were not significantly (<10%) different from those of bulk m-DOM as shown in Table 1, and both exhibited only minor shifts (<12%) throughout the mesocosm experiment when comparing the entire m-DOM,

Table 1 Average mass spectral characteristics of marine dissolved organic samples across bloom experiment comparison to correlated subset data per spectral parameter, weighted by relative intensity

Spectral parameter	H/C	O/C	C/N	MW[a]	n^b
Entire bloom	1.21	0.38	13.0	601.4	10 945
$S_{275-295}$	1.30	0.40	7.2	454.6	266
$S_{350-400}$	1.26	0.38	8.6	509.0	282
ε_{410}	1.34	0.38	8.0	501.6	226

[a] Molecular weight reported here refers to the averaged m/z values measured within each sample. [b] n refers to the number of assigned and unique formulae.

Table 2 Selected classes of compounds that have been shown to be (1) produced naturally in marine environment by microbes and/or (2) have shown to be environmentally relevant photosensitizers characteristics

Mass spectral classification	Major compound types	Representative, naturally-produced analogs	Ref.
Condensed polycyclic aromatic	Aromatic carbonyls	Quinoids[a] 	Ehrhardt *et al.*[c] 1984,[56] Choudhry[b] 1984,[57] Goldstone *et al.*[c] 2000,[58] Wang *et al.*[b] 2020[59]
		Aromatic Ketones/Aldehydes 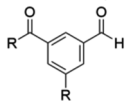	
	Heterocyclic aromatics	Porphyrins[a] 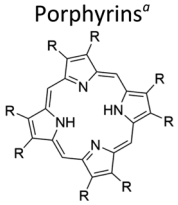	Rottgers *et al.*[b] 2012,[41] D'Ambrosio *et al.*[c] 2020 (ref. 60)
		Flavins/Pterins 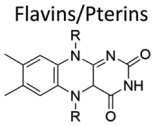	Dunlap *et al.*[b] 1985,[61] Dunlap *et al.*[c] 1986,[62] McNeill *et al.*[c] 2016 (ref. 53)
		Phenols and lignin phenols 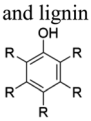	Hernes and Benner[b] 2003,[63] Opsahl *et al.*[c] 1998 (ref. 64)
Polyphenolic	Polyphenolic/aromatic	(A) Flavones/(B) Coumarins/related[a] 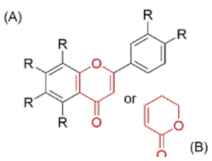	Hartmann *et al.*[b] 2018,[65] Martins *et al.*[b] 2019,[66] McNeill *et al.*[c] 2016 (ref. 53)
Highly unsaturated	Olefins	Linear Terpenoids 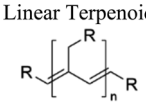	Blunt *et al.*[b] 2010,[67] Medeiros *et al.*[b] 2015,[68] Arakawa *et al.*[b] 2017 (ref. 69)
Aliphatic N+	Amines/amide-like	Amides and peptides[a] 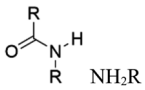	Shields *et al.*[b] 2019,[27] Arnold[c] 2014 (ref. 70)
Aliphatic N−	Carboxyl-rich alicyclic molecules (CRAM)	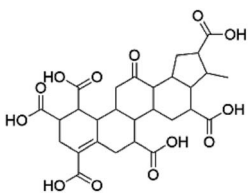	Structure, isomer I, adapted from Hertkorn[b] *et al.* 2006 (ref. 71)

[a] Detected possible structures in m-DOM samples collected from SeaSCAPE 2019 and matched using molecular neural networking. [b] Detected in marine samples. [c] Photosensitizer.

$S_{275-295}$, $S_{350-400}$, ε_{410} subsets. Similar to past studies using electrospray ionization-based mass spectrometry, the intensity-weighted average H/C and O/C ratios of bulk m-DOM were 1.21 and 0.38 respectively.[51] Although, it is important to note that the increase of N, and subsequent decrease of S, could also be due to changes in molecular properties such as acidity or polarity of the analyzed compounds rather than concentration, making them more ionizable by HESI-HRMS. These results reiterate that N may have a key role in this observable pool of m-CDOM in perhaps both structure and its photo-properties, something that has only been recently suggested in literature in comparing the photochemistry of freshwater DOM to marine DOM.[52]

Towards a m-CDOM molecular model

Our efforts to identify and characterize m-CDOM production at the molecular level reveal evidence for autochthonous production of primarily polycyclic, aromatic, and even unsaturated compounds, enriched in N, capable of enhanced light absorbance. Leveraging the controlled mesocosm blooms of the SeaSCAPE 2019 campaign to control for m-CDOM production without ongoing natural or anthropogenic inputs or contamination normally observed in coastal environments, we propose a first step towards molecular models of m-CDOM, and suggest that N-containing structures might also play a role in the photosensitization properties of m-CDOM in the environment – something that has only been recently, and tentatively, posited.[26,29,53] Coupling high resolution mass spectrometry and UV-VIS spectroscopy have allowed for partial molecular-level speciation, advancing from the excitation emission matrix spectroscopy and parallel factor analysis often employed to detect fluorescent components.[22] It should be pointed out that due to the wide ranging complexity of DOM, the inherent biases of methods used to probe composition (such as extraction, pH dependencies, or polarity biases to name a few), remains a challenge in these types of studies. However, the primary focus of this study was to find a subset of representative molecules of m-CDOM even though this may be limited to the specific pool of compounds that were analyzed.

As direct Orbitrap mass spectrometry is not capable of structural analysis, it is recommended that futures studies should employ secondary tandem mass spectrometry, preferably in conjunction with spectroscopic techniques, such as UV-VIS, to single out chromophoric subsets. As such, we analyzed an open-access Orbitrap MS/MS dataset collected from tandem samples taken throughout the SeaSCAPE campaign on the same instrument using the Global Natural Products Social (GNPS) Molecular Networking database.[54] As m-DOM was isolated for MS and MS/MS analyses in identical fashion, comparisons between these parallel datasets are assumed to be viable, with the consideration that MS/MS assignments are capable of identifying structures for only a fraction of detected peaks.

Past studies EI-MS and UV-related measurements, as well as those of statistical determination, of terrestrial DOM show that the signal from negative mode HESI and detectable chromophores in the UV-VIS overlap partially, meaning that many light absorbing compounds in this study are entirely invisible.[55] A review by Mopper and coworkers summarizes the many biases and limitations of techniques used to observe DOM in our environment.[13] Using newer extraction techniques, such as SPE and others, combined with multiple higher resolving techniques inches the scientific community toward a fuller picture of DOM composition. Although our dataset comprises only a fraction of the total, we report thousands of unique molecular formulae. From a fundamental photochemistry perspective, this is quite complex and, thus, molecular models that are representative in both structure and photochemical properties are highly desired. In this study, we attempt to filter these thousands of unique formulae into a few identified structures that may be quite useful for fundamental studies.

In this MS/MS dataset, the GNPS molecular network assigned 586 m-DOM confirmed structural assignments out of the thousands of masses observed throughout the experimental time course examined here. To identify potential m-CDOM candidates within these 586 assignments, Spearman's ranking correlations between peak abundance and the three major spectral parameters of the m-CDOM samples ($S_{350-400}$, $S_{275-295}$, and ε_{410}) were employed, resulting in five, well-correlated ($R > 0.80$) with at least one UV-VIS subset, identified structures (Table 2). Two of these were metal-free, porphyrin-based compounds: coproporphyrin I and III byproducts of heme synthesis and degradation. Of note, other porphyrins were observed in this structurally defined dataset but were not well correlated with the m-CDOM parameters. One of these, pheophorbide A, was observed to weakly correlate ($R = 0.45$) with $S_{350-400}$. The other three structures observed were 5,7-dihydroxyisoflavone, 1,9-hydroxyisorhodoptilometrin, and *N*-phenethylcinnamamide which can be described as a flavone, an anthraquinone/quinoid, and a cinnamamide/aromatic amide, respectively. The mass spectra library matches for each of these compounds can be found in Table S3.† These structures have been detected in marine systems and many of these have been used as photosensitizers (see references in Table 2). Additionally, not only do all of these analog structures absorb in the 275–350 nm regions, there are some such as the porphyrin and flavone/flavin compounds that absorb past 400 nm similar to the UV-VIS absorption of the m-CDOM shown in Fig. 2.[60,62]

Conclusions

Even with a limited number of structures detected due to limitations in known structures of marine organic matter in assignment databases, a molecular picture of m-CDOM begins to emerge from these measurements. We identify an array of structurally diverse marine chromophores, ranging in aromaticity and saturation, many containing N, (Table 2) supporting previous field observations.[72] Some compounds in this analysis are seemingly non-chromophoric, such as aliphatic-like molecules, or non-photosensitizing species like olefins. However, it is important to mention that these classes can have important role in other indirect photochemical mechanisms such as the production of superoxide and radicals or the sink of singlet or triplet state energies.[73,74] Though this table and the classes of compounds identified are largely supported by the results of

this study, it is by no means comprehensive. Even smaller molecular mimics are often desirable for fundamental experimental and theoretical studies to better understand light absorption, environmental factors that effect transition energies and the impacts of light absorbing and non-absorbing compounds within m-DOM. These may include compounds such as 4-benzylbenzoic acid,[74] pyruvic acid,[75] and benzoic acid,[76] as well as possibly more marine relevant[43] and N-containing structures such as imidazole-2-carboxaldehyde.[77] It is important to note that the focus of this study is on discreet molecular entities of light absorbing compounds. Intermolecular (such as donor–acceptor complexes) light absorption involving charge transfer processes is not possible to discern *via* these methods but may also play a role in the properties of m-CDOM.[2,78]

Nevertheless, towards building a realistic model of m-CDOM, in terms of chemical properties and photochemical interactions, this current analysis and combined review of initial compound classes serve as a point of reference for future studies and further characterization. These compounds are, to a certain degree, contrasted to the presumed humic-dominated chromophoric fraction of terrestrial DOM, which has dominated investigations for decades,[79] and highlight the need for further inquiry into this unique fraction of m-DOM. Overall, the findings in this study are important in that they demonstrate the ability to capture composition and insights into structure of at least a portion of the chromophores found in marine waters. Future work incorporating structural-sensitive techniques such as tandem mass spectrometry or NMR[80] with optical spectroscopy, specifically across time-resolved scales, will be needed to take the next steps in understanding the composition and reactivity of m-CDOM.

Author contributions

The manuscript writing was led by MRA, EKC and VHG with contributions and edits from DG, JSS, KM and KAP. Sample collection, data collection and analyses of m-CDOM were led by MRA, EKG, DG and VHG. The SeaSCAPE mesocosm experiment was led by JSS, KM and KAP. All authors have given approval to the final version of the manuscript.

Conflicts of interest

There are no conflicts to declare.

Acknowledgements

The authors gratefully acknowledge the support of the National Science Foundation through the Centers of Chemical Innovation Program *via* the Center for Aerosol Impacts on the Chemistry of the Environment (CHE-1801971) and the National Science Foundation Graduate Research Fellowship Program (DGE-1650112). We acknowledge and thank Vanessa Tian, Duyen Dang, and Professor Michael Tauber for their efforts with m-DOM extraction process and UV-VIS data collection. We would also like to thank Daniel Petras, Tyler Price, Hannah Karp, and the GNPS collaboration for their efforts to establish the open-source Molecular Networking database for SeaSCAPE samples. The SeaSCAPE 2019 campaign would not have been possible without the support from the 50+ person team involved, especially Timothy Bertram, Christopher Cappa, and Christopher Lee for their leadership and organization of the campaign, and the authors would like to thank everyone for their guidance and collaboration.

References

1 D. Hansell, C. Carlson, D. Repeta and R. Schlitzer, Dissolved organic matter in the ocean: a controversy stimulates new insights, *Oceanography*, 2009, **22**, 202–211.
2 C. M. Sharpless and N. V. Blough, The importance of charge-transfer interactions in determining chromophoric dissolved organic matter (CDOM) optical and photochemical properties, *Environ. Sci.: Processes Impacts*, 2014, **16**, 654–671.
3 N. B. Nelson and D. A. Siegel, The global distribution and dynamics of chromophoric dissolved organic matter, *Ann. Rev. Mar. Sci.*, 2013, **5**, 447–476.
4 A. Bricaud, A. Morel and L. Prieur, Absorption by dissolved organic matter of the sea (yellow substance) in the UV and visible domains, *Limnol. Oceanogr.*, 1981, **26**, 43–53.
5 J. I. Hedges, Global biogeochemical cycles: progress and problems, *Mar. Chem.*, 1992, **39**, 67–93.
6 N. Maie, N. M. Scully, O. Pisani and R. Jaffé, Composition of a protein-like fluorophore of dissolved organic matter in coastal wetland and estuarine ecosystems, *Water Res.*, 2007, **41**, 563–570.
7 R. G. Qualls and B. L. Haines, Geochemistry of dissolved organic nutrients in water percolating through a forest ecosystem, *Soil Sci. Soc. Am. J.*, 1991, **55**, 1112–1123.
8 E. J. Rochelle-Newall and T. R. Fisher, Chromophoric dissolved organic matter and dissolved organic carbon in Chesapeake Bay, *Mar. Chem.*, 2002, **77**, 23–41.
9 M. Tzortziou, P. J. Neale, C. L. Osburn, J. P. Megonigal, N. Maie and R. Jaffé, Tidal marshes as a source of optically and chemically distinctive colored dissolved organic matter in the Chesapeake Bay, *Limnol. Oceanogr.*, 2008, **53**, 148–159.
10 K. Mopper, D. J. Kieber and A. Stubbins, in *Biogeochemistry of Marine Dissolved Organic Matter*, Elsevier, 2015, pp. 389–450.
11 C. George, M. Ammann, B. D'Anna, D. J. Donaldson and S. A. Nizkorodov, Heterogeneous photochemistry in the atmosphere, *Chem. Rev.*, 2015, **115**, 4218–4258.
12 K. Stemmler, M. Ammann, C. Donders, J. Kleffmann and C. George, Photosensitized reduction of nitrogen dioxide on humic acid as a source of nitrous acid, *Nature*, 2006, **440**, 195–198.
13 K. Mopper, A. Stubbins, J. D. Ritchie, H. M. Bialk and P. G. Hatcher, Advanced instrumental approaches for characterization of marine dissolved organic matter: Extraction techniques, mass spectrometry, and nuclear magnetic resonance spectroscopy, *Chem. Rev.*, 2007, **107**, 419–442.

14 M. R. Alves, J. S. Sauer, K. A. Prather, V. H. Grassian and C. L. Wilkins, Liquid sampling-atmospheric pressure glow discharge ionization as a technique for the characterization of salt-containing organic samples, *Anal. Chem.*, 2020, **92**, 8845–8851.

15 D. J. Repeta, in *Biogeochemistry of Marine Dissolved Organic Matter*, Elsevier, 2015, pp. 21–63.

16 R. M. Wilson and M. M. Tfaily, Advanced molecular techniques provide new rigorous tools for characterizing organic matter quality in complex systems, *J. Geophys. Res.: Biogeosci.*, 2018, **123**, 1790–1795.

17 B. Lam and A. J. Simpson, Direct 1H NMR spectroscopy of dissolved organic matter in natural waters, *Analyst*, 2008, **133**, 263–269.

18 N. Hertkorn, M. Harir, K. M. Cawley, P. Schmitt-Kopplin and R. Jaffé, Molecular characterization of dissolved organic matter from subtropical wetlands: a comparative study through the analysis of optical properties, NMR and FTICR/MS, *Biogeosciences*, 2016, **13**, 2257–2277.

19 J. I. Hedges, P. G. Hatcher, J. R. Ertel and K. J. Meyers-Schulte, A comparison of dissolved humic substances from seawater with Amazon River counterparts by 13C-NMR spectrometry, *Geochim. Cosmochim. Acta*, 1992, **56**, 1753–1757.

20 M. C. Kido Soule, K. Longnecker, S. J. Giovannoni and E. B. Kujawinski, Impact of instrument and experiment parameters on reproducibility of ultrahigh resolution ESI FT-ICR mass spectra of natural organic matter, *Org. Geochem.*, 2010, **41**, 725–733.

21 Q. Pan, X. Zhuo, C. He, Y. Zhang and Q. Shi, Validation and evaluation of high-resolution orbitrap mass spectrometry on molecular characterization of dissolved organic matter, *ACS Omega*, 2020, **5**, 5372–5379.

22 A. Nebbioso and A. Piccolo, Molecular characterization of dissolved organic matter (DOM): A critical review, *Anal. Bioanal. Chem.*, 2013, **405**, 109–124.

23 E. R. Stabenau and R. G. Zika, Correlation of the absorption coefficient with a reduction in mean mass for dissolved organic matter in southwest Florida river plumes, *Mar. Chem.*, 2004, **89**, 55–67.

24 F. Azam and F. Malfatti, Microbial structuring of marine ecosystems, *Nat. Rev. Microbiol.*, 2007, **5**, 782–791.

25 L. Pomeroy, P. leB. Williams, F. Azam and J. Hobbie, The Microbial Loop, *Oceanography*, 2007, **20**, 28–33.

26 J. D. Kinsey, G. Corradino, K. Ziervogel, A. Schnetzer and C. L. Osburn, Formation of chromophoric dissolved organic matter by bacterial degradation of phytoplankton-derived aggregates, *Front. Mar. Sci.*, 2018, DOI: **10.3389/fmars.2017.00430**.

27 M. R. Shields, T. S. Bianchi, C. L. Osburn, J. D. Kinsey, K. Ziervogel, A. Schnetzer and G. Corradino, Linking chromophoric organic matter transformation with biomarker indices in a marine phytoplankton growth and degradation experiment, *Mar. Chem.*, 2019, **214**, 103665.

28 S. W. Wilhelm and C. A. Suttle, Viruses and nutrient cycles in the sea, *Bioscience*, 1999, **49**, 781–788.

29 J. S. Sauer, K. J. Mayer, C. Lee, M. R. Alves, S. Amiri, C. J. Bahaveolos, E. B. Franklin, D. R. Crocker, D. Dang, J. Dinasquet, L. A. Garofalo, C. P. Kaluarachchi, D. B. Kilgour, L. E. Mael, B. A. Mitts, D. R. Moon, A. N. Moore, C. K. Morris, C. A. Mullenmeister, C. M. Ni, M. A. Pendergraft, D. Petras, R. M. C. Simpson, S. Smith, P. R. Tumminello, J. L. Walker, P. J. Demott, D. K. Farmer, A. H. Goldstein, V. H. Grassian, J. S. Jaffe, F. Malfatti, T. R. Martz, J. H. Slade, A. V. Tivanski, T. H. Bertram, C. D. Cappa and K. A. Prather, The Sea Spray Chemistry and Particle Evolution study (SeaSCAPE): Overview and experimental methods, *Environ. Sci.: Processes Impacts*, 2022, **24**, 290–315.

30 A. Stubbins, J. Niggemann and T. Dittmar, Photo-lability of deep ocean dissolved black carbon, *Biogeosciences*, 2012, **9**, 1661–1670.

31 T. Dittmar, B. Koch, N. Hertkorn and G. Kattner, A simple and efficient method for the solid-phase extraction of dissolved organic matter (SPE-DOM) from seawater, *Limnol. Oceanogr.: Methods*, 2008, **6**, 230–235.

32 J. R. Helms, A. Stubbins, J. D. Ritchie, E. C. Minor, D. J. Kieber and K. Mopper, Absorption spectral slopes and slope ratios as indicators of molecular weight, source, and photobleaching of chromophoric dissolved organic matter, *Limnol. Oceanogr.*, 2008, **53**, 955–969.

33 E. K. Coward, T. Ohno and D. L. Sparks, Direct evidence for temporal molecular fractionation of dissolved organic matter at the iron oxyhydroxide interface, *Environ. Sci. Technol.*, 2019, **53**, 642–650.

34 T. Ohno and P. E. Ohno, Influence of heteroatom pre-selection on the molecular formula assignment of soil organic matter components determined by ultrahigh resolution mass spectrometry, *Anal. Bioanal. Chem.*, 2013, **405**, 3299–3306.

35 B. P. Koch and T. Dittmar, From mass to structure: An aromaticity index for high-resolution mass data of natural organic matter, *Rapid Commun. Mass Spectrom.*, 2006, **20**, 926–932.

36 P. Herzsprung, W. Von Tümpling, N. Hertkorn, M. Harir, O. Büttner, J. Bravidor, K. Friese and P. Schmitt-Kopplin, Variations of DOM quality in inflows of a drinking water reservoir: Linking of van krevelen diagrams with EEMF spectra by rank correlation, *Environ. Sci. Technol.*, 2012, **46**, 5511–5518.

37 J. R. Helms, A. Stubbins, E. M. Perdue, N. W. Green, H. Chen and K. Mopper, Photochemical bleaching of oceanic dissolved organic matter and its effect on absorption spectral slope and fluorescence, *Mar. Chem.*, 2013, **155**, 81–91.

38 X. Wang, C. M. Sultana, J. Trueblood, T. C. J. Hill, F. Malfatti, C. Lee, O. Laskina, K. A. Moore, C. M. Beall, C. S. McCluskey, G. C. Cornwell, Y. Zhou, J. L. Cox, M. A. Pendergraft, M. V. Santander, T. H. Bertram, C. D. Cappa, F. Azam, P. J. DeMott, V. H. Grassian and K. A. Prather, Microbial control of sea spray aerosol composition: A tale of two blooms, *ACS Cent. Sci.*, 2015, **1**, 124–131.

39 C. Lee, C. M. Sultana, D. B. Collins, M. V. Santander, J. L. Axson, F. Malfatti, G. C. Cornwell, J. R. Grandquist, G. B. Deane, M. D. Stokes, F. Azam, V. H. Grassian and K. A. Prather, Advancing model systems for fundamental laboratory studies of sea spray aerosol using the microbial loop, *J. Phys. Chem. A*, 2015, **119**, 8860–8870.

40 L. C. Powers, R. Del Vecchio, N. V. Blough, N. McDonald, P. Schmitt-Kopplin and M. Gonsior, Optical properties and photochemical transformation of the dissolved organic matter released by Sargassum, *Front. Mar. Sci.*, 2020, **7**, DOI: **10.3389/fmars.2020.588287**.

41 R. Röttgers and B. P. Koch, Spectroscopic detection of a ubiquitous dissolved pigment degradation product in subsurface waters of the global ocean, *Biogeosciences*, 2012, **9**, 2585–2596.

42 A. A. Andrew, R. Del Vecchio, A. Subramaniam and N. V. Blough, Chromophoric dissolved organic matter (CDOM) in the Equatorial Atlantic Ocean: Optical properties and their relation to CDOM structure and source, *Mar. Chem.*, 2013, **148**, 33–43.

43 N. V. Karimova, M. R. Alves, M. Luo, V. H. Grassian and R. B. Gerber, Toward a microscopic model of light absorbing dissolved organic compounds in aqueous environments: theoretical and experimental study, *Phys. Chem. Chem. Phys.*, 2021, **23**, 10487–10497.

44 A. Seritti, E. Morelli, L. Nannicini and R. Del Vecchio, Production of hydrophobic fluorescent organic matter by the marine diatom Phaeodactylum tricornutum, *Chemosphere*, 1994, **28**, 117–129.

45 C. A. Stedmon and N. B. Nelson, *The Optical Properties of DOM in the Ocean*, Elsevier Inc., 2nd edn, 2015.

46 E. A. Vialykh, G. Mckay and F. L. Rosario-Ortiz, Computational assessment of the three-dimensional configuration of dissolved organic matter chromophores and influence on absorption spectra, *Environ. Sci. Technol.*, 2020, **54**, 15904–15913.

47 R. H. John, A. Stubbins, J. D. Ritchie, E. C. Minor, D. J. Kieber and K. Mopper, Erratum: Absorption spectral slopes and slope ratios as indicators of molecular weight, source, and photobleaching of chromophoric dissolved organic matter (Limnology and Oceanography 53 955-969, *Limnol. Oceanogr.*, 2009, **54**, 1023.

48 H. Chen, B. Zheng, Y. Song and Y. Qin, Correlation between molecular absorption spectral slope ratios and fluorescence humification indices in characterizing CDOM, *Aquat. Sci.*, 2011, **73**, 103–112.

49 R. Benner, B. Biddanda, B. Black and M. McCarthy, Abundance, size distribution, and stable carbon and nitrogen isotopic compositions of marine organic matter isolated by tangential-flow ultrafiltration, *Mar. Chem.*, 1997, **57**, 243–263.

50 M. D. McCarthy, J. I. Hedges and R. Benner, Major bacterial contribution to marine dissolved organic nitrogen, *Science*, 1998, **281**, 231–234.

51 E. B. Kujawinski, K. Longnecker, K. L. Barott, R. J. M. Weber and M. C. K. Soule, Microbial community structure affects marine dissolved organic matter composition, *Front. Mar. Sci.*, 2016, **3**, 1–15.

52 L. T. Stirchak, K. J. Moor, K. McNeill and D. J. Donaldson, Differences in photochemistry between seawater and freshwater for two natural organic matter samples, *Environ. Sci.: Processes Impacts*, 2019, 28–39.

53 K. McNeill and S. Canonica, Triplet state dissolved organic matter in aquatic photochemistry: Reaction mechanisms, substrate scope, and photophysical properties, *Environ. Sci.: Processes Impacts*, 2016, **18**, 1381–1399.

54 M. Wang, J. J. Carver, V. V. Phelan, L. M. Sanchez, N. Garg, Y. Peng, D. D. Nguyen, J. Watrous, C. A. Kapono, T. Luzzatto-Knaan, C. Porto, A. Bouslimani, A. V. Melnik, M. J. Meehan, W. T. Liu, M. Crüsemann, P. D. Boudreau, E. Esquenazi, M. Sandoval-Calderón, R. D. Kersten, L. A. Pace, R. A. Quinn, K. R. Duncan, C. C. Hsu, D. J. Floros, R. G. Gavilan, K. Kleigrewe, T. Northen, R. J. Dutton, D. Parrot, E. E. Carlson, B. Aigle, C. F. Michelsen, L. Jelsbak, C. Sohlenkamp, P. Pevzner, A. Edlund, J. McLean, J. Piel, B. T. Murphy, L. Gerwick, C. C. Liaw, Y. L. Yang, H. U. Humpf, M. Maansson, R. A. Keyzers, A. C. Sims, A. R. Johnson, A. M. Sidebottom, B. E. Sedio, A. Klitgaard, C. B. Larson, C. A. P. Boya, D. Torres-Mendoza, D. J. Gonzalez, D. B. Silva, L. M. Marques, D. P. Demarque, E. Pociute, E. C. O'Neill, E. Briand, E. J. N. Helfrich, E. A. Granatosky, E. Glukhov, F. Ryffel, H. Houson, H. Mohimani, J. J. Kharbush, Y. Zeng, J. A. Vorholt, K. L. Kurita, P. Charusanti, K. L. McPhail, K. F. Nielsen, L. Vuong, M. Elfeki, M. F. Traxler, N. Engene, N. Koyama, O. B. Vining, R. Baric, R. R. Silva, S. J. Mascuch, S. Tomasi, S. Jenkins, V. Macherla, T. Hoffman, V. Agarwal, P. G. Williams, J. Dai, R. Neupane, J. Gurr, A. M. C. Rodríguez, A. Lamsa, C. Zhang, K. Dorrestein, B. M. Duggan, J. Almaliti, P. M. Allard, P. Phapale, L. F. Nothias, T. Alexandrov, M. Litaudon, J. L. Wolfender, J. E. Kyle, T. O. Metz, T. Peryea, D. T. Nguyen, D. VanLeer, P. Shinn, A. Jadhav, R. Müller, K. M. Waters, W. Shi, X. Liu, L. Zhang, R. Knight, P. R. Jensen, B. Palsson, K. Pogliano, R. G. Linington, M. Gutiérrez, N. P. Lopes, W. H. Gerwick, B. S. Moore, P. C. Dorrestein and N. Bandeira, Sharing and community curation of mass spectrometry data with Global Natural Products Social Molecular Networking, *Nat. Biotechnol.*, 2016, **34**, 828–837.

55 J. A. Hawkes, P. J. R. Sjöberg, J. Bergquist and L. J. Tranvik, Complexity of dissolved organic matter in the molecular size dimension: Insights from coupled size exclusion chromatography electrospray ionisation mass spectrometry, *Faraday Discuss.*, 2019, **218**, 52–71.

56 M. Ehrhardt and G. Petrick, On the sensitized photo-oxidation of alkylbenzenes in seawater, *Mar. Chem.*, 1984, **15**, 47–58.

57 G. G. Choudhry, in *Handbook of Environmental Chemistry*, 1984, vol. 1, pp. 1–24.

58 J. V. Goldstone and B. M. Voelker, Chemistry of superoxide radical in seawater: CDOM associated sink of superoxide in coastal waters, *Environ. Sci. Technol.*, 2000, **34**, 1043–1048.

59 Y. Wang and J. Ma, Quantitative determination of redox-active carbonyls of natural dissolved organic matter, *Water Res.*, 2020, **185**, 116142.
60 M. D'Ambrosio, A. C. Santos, A. Alejo-Armijo, A. J. Parola and P. M. Costa, Light-mediated toxicity of porphyrin-like pigments from a marine polychaeta, *Mar. Drugs*, 2020, **18**, 1–14.
61 W. C. Dunlap and M. Susic, Determination of pteridines and flavins in seawater by reverse-phase, high-performance liquid chromatography with fluorometric detection, *Mar. Chem.*, 1985, **17**, 185–198.
62 W. C. Dunlap and M. Susic, Photochemical decomposition rates of pteridines and flavins in seawater exposed to surface solar radiation, *Mar. Chem.*, 1986, **19**, 99–107.
63 P. J. Hernes, Photochemical and microbial degradation of dissolved lignin phenols: Implications for the fate of terrigenous dissolved organic matter in marine environments, *J. Geophys. Res.*, 2003, **108**, 3291.
64 S. Opsahl and R. Benner, Photochemical reactivity of dissolved lignin in river and ocean waters, *Limnol. Oceanogr.*, 1998, **43**, 1297–1304.
65 A. Hartmann, M. Ganzera, U. Karsten, A. Skhirtladze and H. Stuppner, Phytochemical and analytical characterization of novel sulfated coumarins in the marine green macroalga Dasycladus vermicularis (Scopoli) Krasser, *Molecules*, 2018, **23**, 2735.
66 B. T. Martins, M. Correia da Silva, M. Pinto, H. Cidade and A. Kijjoa, Marine natural flavonoids: chemistry and biological activities, *Nat. Prod. Res.*, 2019, **33**, 3260–3272.
67 J. W. Blunt, B. R. Copp, M. H. G. Munro, P. T. Northcote and M. R. Prinsep, Marine natural products, *Nat. Prod. Rep.*, 2010, **27**, 165–237.
68 P. M. Medeiros, M. Seidel, L. C. Powers, T. Dittmar, D. A. Hansell and W. L. Miller, Dissolved organic matter composition and photochemical transformations in the northern North Pacific Ocean, *Geophys. Res. Lett.*, 2015, **42**, 863–870.
69 N. Arakawa, L. I. Aluwihare, A. J. Simpson, R. Soong, B. M. Stephens and D. Lane-Coplen, Carotenoids are the likely precursor of a significant fraction of marine dissolved organic matter, *Sci. Adv.*, 2017, **3**, 1–12.
70 W. A. Arnold, One electron oxidation potential as a predictor of rate constants of N-containing compounds with carbonate radical and triplet excited state organic matter, *Environ. Sci.: Processes Impacts*, 2014, **16**, 832–838.
71 N. Hertkorn, R. Benner, M. Frommberger, P. Schmitt-Kopplin, M. Witt, K. Kaiser, A. Kettrup and J. I. Hedges, Characterization of a major refractory component of marine dissolved organic matter, *Geochim. Cosmochim. Acta*, 2006, **70**, 2990–3010.
72 E. J. Biers, R. G. Zepp and M. A. Moran, The role of nitrogen in chromophoric and fluorescent dissolved organic matter formation, *Mar. Chem.*, 2007, **103**, 46–60.
73 X. Wang, E. Z. Dalton, Z. C. Payne, S. Perrier, M. Riva, J. D. Raff and C. George, Superoxide and nitrous acid production from nitrate photolysis is enhanced by dissolved aliphatic organic matter, *Environ. Sci. Technol. Lett.*, 2021, **8**, 53–58.
74 J. V. Trueblood, M. R. Alves, D. Power, M. V. Santander, R. E. Cochran, K. A. Prather and V. H. Grassian, Shedding light on photosensitized reactions within marine-relevant organic thin films, *ACS Earth Space Chem.*, 2019, **3**, 1614–1623.
75 D. Shemesh, M. Luo, V. H. Grassian and R. B. Gerber, Absorption spectra of pyruvic acid in water: insights from calculations for small hydrates and comparison to experiment, *Phys. Chem. Chem. Phys.*, 2020, **22**, 12658–12670.
76 N. V. Karimova, M. Luo, V. H. Grassian and R. Benny Gerber, Absorption spectra of benzoic acid in water at different pH and in the presence of salts: Insights from the integration of experimental data and theoretical cluster models, *Phys. Chem. Chem. Phys.*, 2020, **22**, 5046–5056.
77 L. González Palacios, P. Corral Arroyo, K. Z. Aregahegn, S. S. Steimer, T. Bartels-Rausch, B. Nozière, C. George, M. Ammann and R. Volkamer, Heterogeneous photochemistry of imidazole-2-carboxaldehyde: HO_2 radical formation and aerosol growth, *Atmos. Chem. Phys.*, 2016, **16**, 11823–11836.
78 G. McKay, J. A. Korak, P. R. Erickson, D. E. Latch, K. McNeill and F. L. Rosario-Ortiz, The case against charge transfer interactions in dissolved organic matter photophysics, *Environ. Sci. Technol.*, 2018, **52**, 406–414.
79 G. McKay, Emerging investigator series: Critical review of photophysical models for the optical and photochemical properties of dissolved organic matter, *Environ. Sci.: Processes Impacts*, 2020, **22**, 1139–1165.
80 M. Seidel, S. P. B. Vemulapalli, D. Mathieu and T. Dittmar, Marine dissolved organic matter shares thousands of molecular formulae yet differs structurally across major water masses, *Environ. Sci. Technol.*, 2022, **56**, 3758–3769.